Hot isostatic pressing of laser powder bed fusion AlSi10Mg: parameter identification and mechanical properties

Juan Guillermo Santos Macías[1], Lv Zhao[2], David Tingaud[3], Brigitte Bacroix[3], Grzegorz Pyka[1], Camille van der Rest[1], Laurence Ryelandt[1], Aude Simar[1,*]

[1] *Université catholique de Louvain, Institute of Mechanics, Materials and Civil Engineering, IMAP, B-1348 Louvain la Neuve, Belgium*

[2] *Huazhong University of Science and Technology, School of Aerospace Engineering, Department of Mechanics, Wuhan, China*

[3] *Université Sorbonne Paris Nord, Laboratoire des Sciences des Procédés et des Matériaux, CNRS, UPR 3407, Villetaneuse, 93430, France*

[*] Corresponding author. Email address: aude.simar@uclouvain.be

Abstract

The fatigue crack initiation of as built (AB) laser powder bed fusion (LPBF) AlSi10Mg is highly affected by the presence of large porosities inherent to the process. Hot isostatic pressing (HIP) is a potential means of reduction of this detrimental porosity. Classic high temperature HIP treatments at about 500°C and 100 MPa pressure lead to significant strength loss that is partially recovered after additional solution and ageing heat treatments, i.e. overall a three-step treatment. In this work, a 350°C HIP treatment performed under a higher pressure of 300 MPa for 2 hours has been identified as a promising post-treatment for LPBF AlSi10Mg using finite element method simulations of the HIP process. This treatment is shown to suppress these large porosities and lead to higher fracture strain and total fatigue life than after the classic three-step treatment (HIP + two steps of heat treatment). Both HIP treatments also present higher fracture strain compared to the AB material. Thus, this new 350°C HIP treatment efficiently removes the need for post-treatments after HIP. The 350°C at 300MPa HIP treatment improves the yield strength weighted fatigue resistance compared to the AB material but not the absolute fatigue life.

Keywords: Laser powder bed fusion, AlSi10Mg, hot isostatic pressing, X-ray tomography, total fatigue life

1. Introduction

Laser powder bed fusion (LPBF) of AlSi10Mg is a promising process allowing to produce parts with a high complexity without any additional cost [1]. This process attracts the aerospace industry for the production of specific parts presenting limited need for material but enhanced complexity. Aluminium alloys are also attractive materials for this industry as they present a high strength to weight ratio. AlSi10Mg is a common aluminium alloy extensively studied for the LPBF process [2]. Now, most parts for this industry have additional requirements in terms of mechanical properties, including strength, ductility and resistance to fatigue loading.

Ductility of LPBF AlSi10Mg in the as built (AB) condition is rather low [3] and can be improved significantly by applying post-treatments, including the common stress relieve heat treatment [3,4]. It is also well known [4-8] that porosity is the main reason for fatigue crack nucleation in LPBF AlSi10Mg. For this reason, hot isostatic pressing (HIP) post-treatments are generally envisioned aiming at porosity reduction. HIP involves a combination of high temperature and pressure generally applied by an argon gas [9]. Such post-treatments are very effective in increasing fatigue life of LPBF Ti6Al4V titanium alloys [10].

For aluminium alloys, the classic HIP treatment is applied at 500°C under a pressure of 100 MPa [9]. However, there are limited number of published results treating the HIP of LPBF AlSi10Mg [11-23] and only a few of them addressed the effect of HIP on fatigue resistance.

Rosenthal et al. [11] examined the effect of HIP on the AlSi10Mg produced by LPBF comparing with the effect of heat treatments. In that study, several samples underwent HIP during 1 h under a pressure of 100 MPa and a temperature of 330°C or 530°C. These cycles were compared with a heat treatment carried out during 2.5 hours at 540°C. The resulting mechanical properties are always inferior for the treated samples compared to the as built samples except for a higher elongation at failure. Rosenthal et al. [11] concluded that these differences are due to the globularisation and coarsening of the very fine structure of silicon-rich eutectic after heat treatment. Hirata et al. [12] performed HIP (500°C, 100 MPa, 2 hours) followed by solution treatment (500°C for 2 hours) and reached the same conclusion about the Si network influence on the alloy's strength. Rosenthal et al. [11] also concluded that the tensile properties are quite equivalent between the HIP cycle at 530°C and the heat treatment at 540° C. The pressure of 100 MPa thus played only a very minor role during this HIP cycle. Rosenthal

et al. [13] have compared the effects of a modified T5 heat treatment (2h, 200°C) and a 2h HIP treatment at 100 MPa and 500°C for the LPBF AlSi10Mg. The tensile strength of samples heat treated at 200°C is quite close to that of as built samples, but the strength after HIP at 500°C is very low.

Uzan et al. [14] also investigated the effect of HIP treatments following a stress relieve heat treatment (300°C for 2 hours). This study is building on the results obtained by Rosenthal et al. [11] as they identified that a pressure of 100 MPa was insufficient in a HIP cycle and thus increased it to 180 MPa. The complete parameters of the HIP cycles carried out are 2 h under 180 MPa at 250°C or 500°C. The 250°C HIP treatment affected only marginally the tensile properties compared to a classical stress relief heat treatment (300°C / 2 hours). The fatigue strength of the samples after stress relieve and HIP at 250°C is slightly lower than that of the samples after stress relieve. In addition, the samples after HIP at 500°C have the lowest fatigue strength of all.

Finfrock et al. [15] applied HIP at 521°C under 103 MPa pressure for 2 hours. They also showed a reduction of porosity and strength compared to the as built material. They associated the scatter in ductility of hot isostatic pressed parts to the presence of unclosed surface porosities facilitating crack nucleation.

Several studies attempted to alleviate HIP induced strength loss through subsequent precipitation heat treatments [16-21]. Tradowsky et al. [16] applied a HIP process at 530°C under 100 MPa pressure for 2 hours after LPBF of AlSi10Mg followed by a T6 treatment (solution followed by ageing treatment). Again, porosity reduction was clearly identified. The loss of strength due to the HIP treatment was partly compensated by the T6 treatment. Ertuğrul et al. [17] compared HIP (500°C / 100 MPa), HIP + T6 treatment with different ageing durations (540°C solution treatment + 180°C during 4h or 12h) and T6 treatment on stress relieved samples. It was found that the HIP process could effectively reduce porosity, the HIP + T6 treatment leading to higher strength and ductility than the T6 condition. Larrosa et al. [18] applied the same HIP followed by T6 treatment as [16] and analysed their samples under X-ray tomography. They have shown a statistically analysed 44 to 65% reduction in porosity. The fatigue life seems to be dominated by the presence of crack-like (pancake-like) defects, similarly to what Finfrock et al. [15] identified. Recently, Hastie et al. [19,20] have further analysed the porosity distribution using X-ray tomography for similar HIP followed by T6 treatment clearly showing closing and flattening of pores of an equivalent diameter larger than

50 µm. They also showed that the subsequent T6 treatment [19] or tensile loading [20] cause pores to reopen back to their original shape, but still with overall densification.

Other fatigue data are provided by Kan et al. [21] also on the HIP (520°C/100MPa/2 hours) followed by T6 treatment, which was found ineffective in closing pores, showing only marginal improvement in fatigue life compared to the selected reference stress relieve treatment (210°C for 1 hour). Contrastingly, Schneller et al. [22,23] obtained a small fatigue life enhancement after a HIP (500°C / 100 MPa / 2 hours) followed by T6 treatment.

Recently, Tocci et al. [24] and Giovagnoli et al. [25] modified the traditional route of HIP + T6 presented above, designating the new HPT6 high-pressure T6 treatment. The HPT6 route combines HIP, gas quenching and ageing at high pressures, thus cutting down processing duration and cost. HPT6 was demonstrated to effectively densify LPBF AlSi10Mg and promote precipitation strengthening, leading to similar mechanical performance (strength and ductility) to that of a standard HIP + T6 route. Nevertheless, no fatigue data was reported to show the influence of HPT6 on fatigue resistance.

Thus, the current state of the art of HIP treatments of LPBF AlSi10Mg is clearly not showing the same impressive improvement in fatigue life observed in titanium alloys. This is expectedly due to significant yield strength loss associated to the high temperature of HIP. In the present study, a finite element model allowed to identify HIP at 350°C as potentially interesting. After an experimental confirmation of the simulation results, tensile and fatigue properties are compared for three conditions: as built, HIP at 350°C and HIP followed by a two-step T6 solution and ageing treatment, this last having been shown by the preceding literature review to be the classic treatment. The new HIP at 350°C treatment leads to higher fracture strain and total fatigue life than the HIP at 500°C followed by T6. However, both HIP treatments still lead to a reduction of fatigue resistance and strength, but produces better results than the classic HIP treatment. In addition, fracture strain is enhanced compared to the as built material.

2. Simulation method and results

To help in the determination of sound HIP parameters specific to LPBF AlSi10Mg, a numerical simulation of porosity evolution with HIP was performed using an elasto-viscoplastic model built with Abaqus [26]. Three analysis steps were created in the simulation. The first one was devoted to applying hydrostatic pressure, which was then maintained in the second step to

simulate the creep material flow at high temperature. Finally the pressure was removed in the third step and the porosity after HIP was determined. The representative volume element is illustrated in Fig. 1, featuring a 50 µm pore at the centre of a 403 µm side cube that represents an initial porosity occupying 0.1 % of the volume. This porosity level is representative of the porosity observed experimentally in as built conditions when observed at high tomography resolution (0.75 µm), as reported in previous work [4]. Periodic boundary conditions and isostatic pressure were applied on the outer surfaces. The model contained 5480 solid elements with reduced integration (C3D8R). The mesh was locally refined in the region around the pore to reliably capture the pore size reduction (see Fig. 1b). A finer mesh could be useful to increase the accuracy of simulations, however, it would lead to much higher computational costs and convergence issues. At the current stage, the aforementioned mesh was used to study the porosity reduction trend when using different HIP parameter sets.

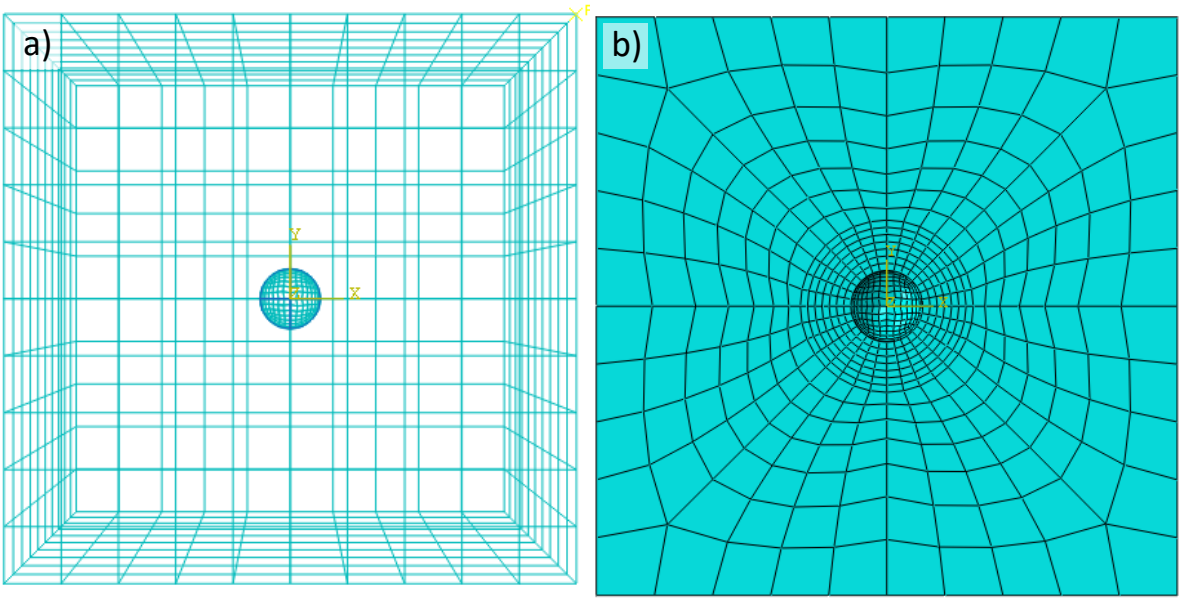

Fig. 1 Representative volume element for the finite element method model. The 50 µm pore at the centre occupies 0.1 % of the total volume (a). The mesh is refined around the pore (b)

A pressure holding time of 2 h was systematically applied. Temperatures of 250°C, 300°C, 350°C and 400°C and pressures of 100 MPa, 150 MPa, 200 MPa, 250 MPa, 300 MPa and 350MPa were selected. The material properties at high temperature (including creep properties) for LPBF AlSi10Mg, presented in supplementary Table 1, were procured from Uzan et al. [27]. Only steady-state regime was considered, with constant strain rate expressed as $\dot{\tilde{\varepsilon}}^{cr} = A\tilde{q}^n$, where constant A depends on thermal activation energy and temperature, $\tilde{q}$ is the effective

deviatoric stress and *n* is another constant [26]. *A* and *n* were fitted with experimental data reported in [27]. The obtained results are plotted in Fig. 2. All HIP conditions reduce porosity, but not in a significant way for the 250°C and 300°C parameter sets. Contrastingly, at a HIP temperature of 350°C, the porosity is very notably reduced when using a pressure equal or larger than 150 MPa. Moreover, the simulation results revealed that the densification was mainly achieved during the application of high temperature and hydrostatic pressure, while the creep state represented limited contribution. In this sense, the significant porosity reduction above 350°C is mainly due to the rapid yield strength decrease at high temperature (see supplementary Table 1). These predictions were confronted to experimental results. A reference pressure of 300 MPa offering a good compromise was chosen.

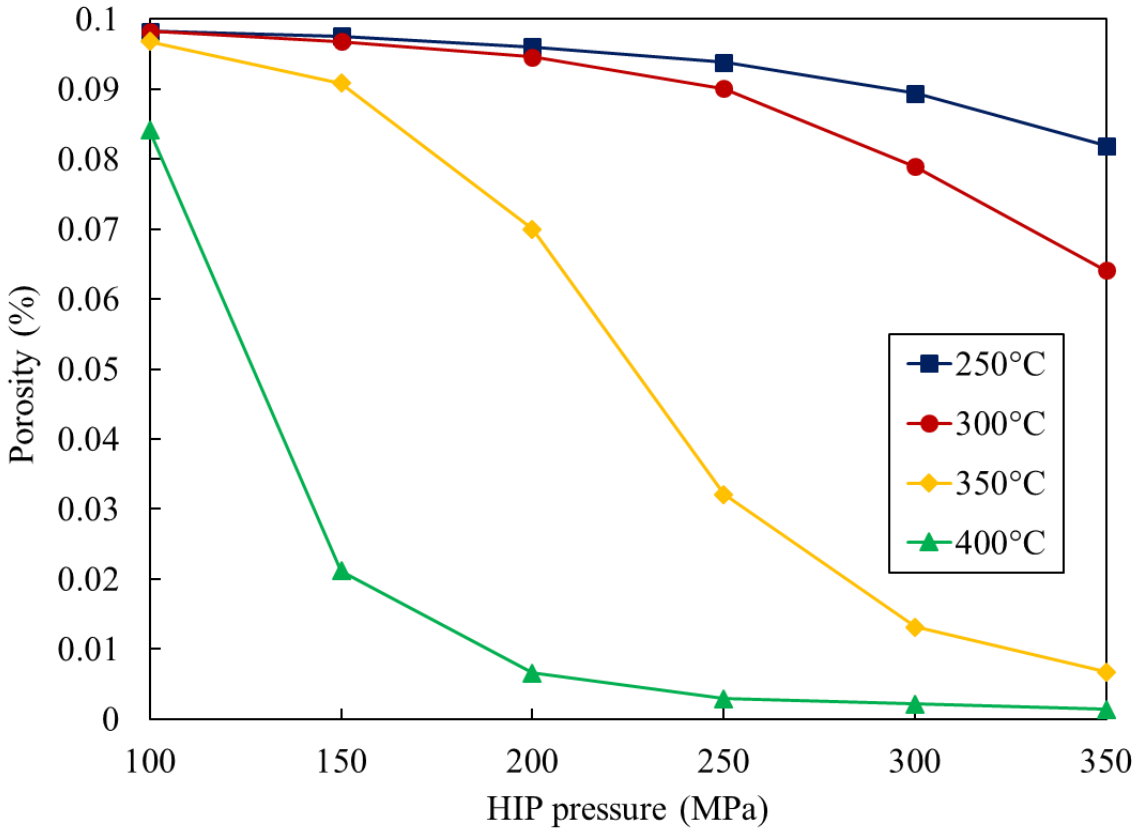

Fig. 2 Finite element simulation of porosity reduction with varying HIP pressure and temperature (applied during 2 hours)

3. Experimental methods

The material used in this study was produced by laser powder bed fusion of AlSi10Mg alloy with an EOS M290 machine, a build platform temperature of 35°C, under argon gas and the following parameters optimised by the machine manufacturer [28]: Power of 390 W, scanning speed of 1300 mm/s, hatch spacing of 190 µm, layer thickness of 30 µm, scan rotation of 67°. Vertically oriented 5 mm diameter and 70 mm long cylinders were built.

As built LPBF AlSi10Mg samples were post-treated by hot isostatic pressing at Université Sorbonne Paris Nord (Villetaneuse, France). The furnace is pictured in Fig. 3. This process is characterised by the application of isostatic pressure through argon gas at a certain temperature during a determined amount of time, as exemplified in Fig. 4.

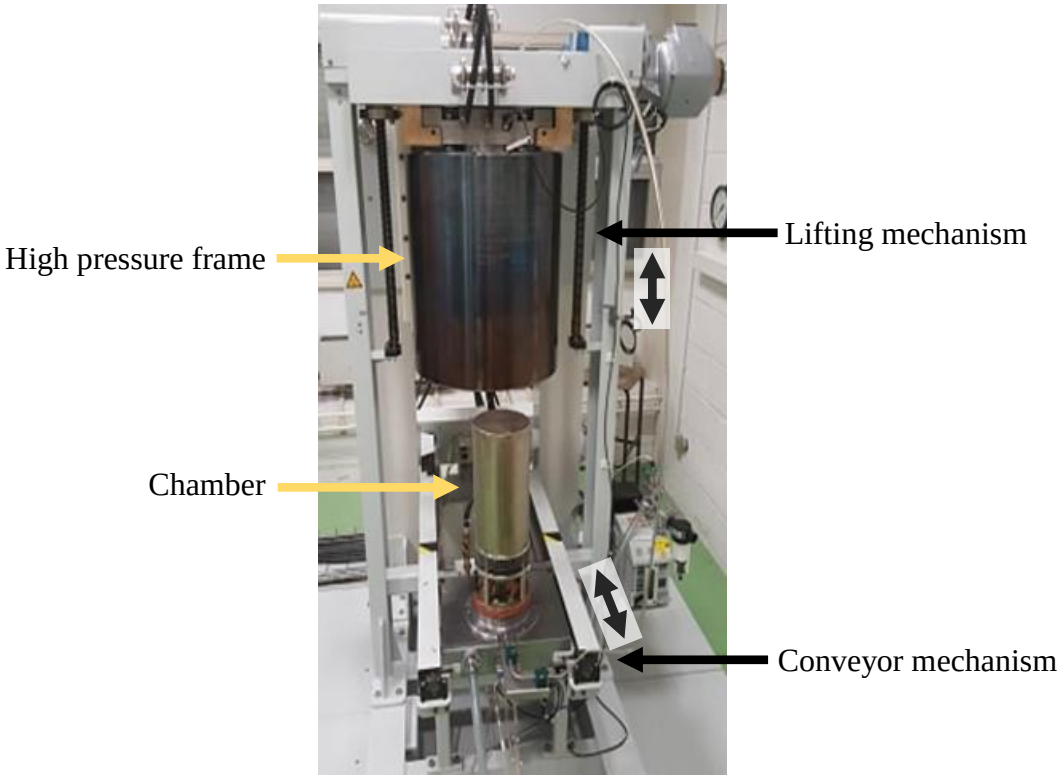

Fig. 3 Hot isostatic pressing furnace

The different HIP parameters studied in this work are provided in Table 1. The denomination of the various conditions include the HIP temperature and, when the pressure or the time is different to 300 MPa and 2 h, a second number to specify modified HIP treatment time or pressure, except for HIP 497 since it is the only condition at 497°C.

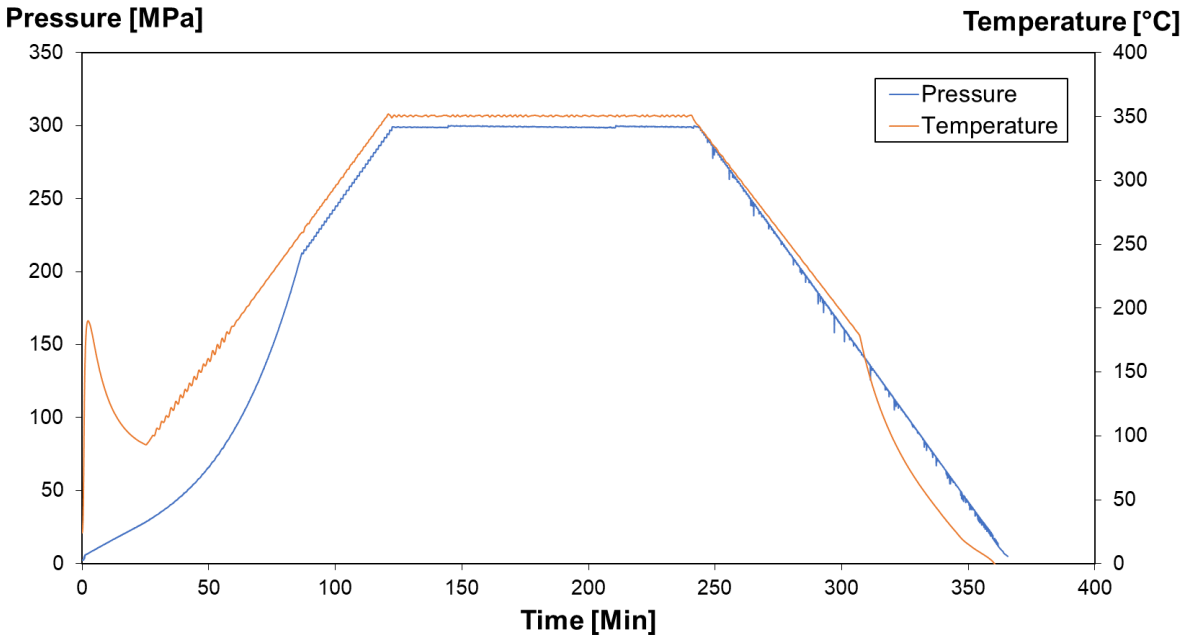

Fig. 4 Example of a HIP cycle when aiming for a temperature of 350°C and a pressure of 300 MPa

Considering the severe depletion of strength after classic HIP at a temperature around 500°C, the HIP 497 material underwent solution heat treatment at 540°C during 3 h, with a quench in water at 50°C, followed by artificial ageing at 200°C during 8 h, corresponding to a T6 post-treatment. This HIP + T6 treatment is recommended in literature, but with slightly different parameters [16,18]. The same 200°C ageing treatment was also performed in samples of HIP 350 material, as well as an alternative one at 160°C, followed by HV0.2 hardness measurements using an EMCO-TEST durascan 70 G5 machine.

Table 1. HIP parameters.

Denomination	Temperature	Pressure	Time
HIP 300	300°C	300 MPa	2 h
HIP 300 - 4 h	300°C	300 MPa	4 h
HIP 300 - 100 MPa	300°C	100 MPa	2 h
HIP 350	350°C	300 MPa	2 h
HIP 497	497°C	100 MPa	2 h

Porosity determination to check the densification effect of HIP was achieved through laboratory X-ray computed tomography with 1.66 µm voxel size, performed using a GE Phoenix nanotom m system on AB and post-treated material. To ascertain the homogeneity of the post-treatment, two scans were conducted on different locations in the length of a cylinder after HIP at 350°C (at 300 MPa for 2 h).

Scanning electron microscopy (SEM) on a Zeiss FEG-SEM ultra 55 microscope allowed to characterise selected specimens. Samples were finely polished and etched with Struers active oxide polishing suspension and a 0.5 vol% HF solution prior to observation.

Uniaxial tensile testing was carried out on a 50 kN Zwick/Roell ProLine universal testing machine following ASTM E8/E8M - 15a standard to characterise the static mechanical behaviour of as built and post-processed samples. Round tensile specimens were machined from the initial cylinders (see Fig. 5). At least three specimens were tested for each condition. Certain samples were cut in half longitudinally after failure to perform damage characterisation using SEM following materialographic preparation.

Fig. 5 Geometry of tensile and fatigue testing samples extracted from vertically built LPBF cylinders

To study the cyclic behaviour of the more interesting conditions, force controlled constant amplitude axial tensile-tensile fatigue testing was performed according to ASTM E466 - 15 standard on a 25 kN MTS Bionix servohydraulic test system, with $R = \sigma_{min}/\sigma_{max} = 0.1$ and f = 30 Hz. The round geometry of the specimens is represented in Fig. 5. The samples were polished to reduce roughness below a R_a of 0.1 µm. SEM fractography was carried out on failed specimens to identify the origin of the failure.

4. Results

4.1. Process parameter selection using porosity

The porosity data obtained from the tomography scans are presented in 3D for the samples containing detectable porosity levels for the selected resolution (AB, 300°C HIP and 497°C HIP + T6 conditions) in Fig. 6a-e, along with the cumulative pore size distribution (Fig. 6f). Data for all considered states are provided in Table 2. Samples HIP 350°C and HIP 497°C are not included in Fig. 6 since no significant porosity is observed in these states (see supplementary Fig 1). The AB material presents a density level well above 99.5% that is in the expected range for LPBF AlSi10Mg. Note however that the selected X-ray tomography resolution (1.66 µm voxel size) does not allow identifying small porosities. Nevertheless, smaller porosities would

affect density but are not expected to be a source of fatigue crack initiation in the presence of larger ones.

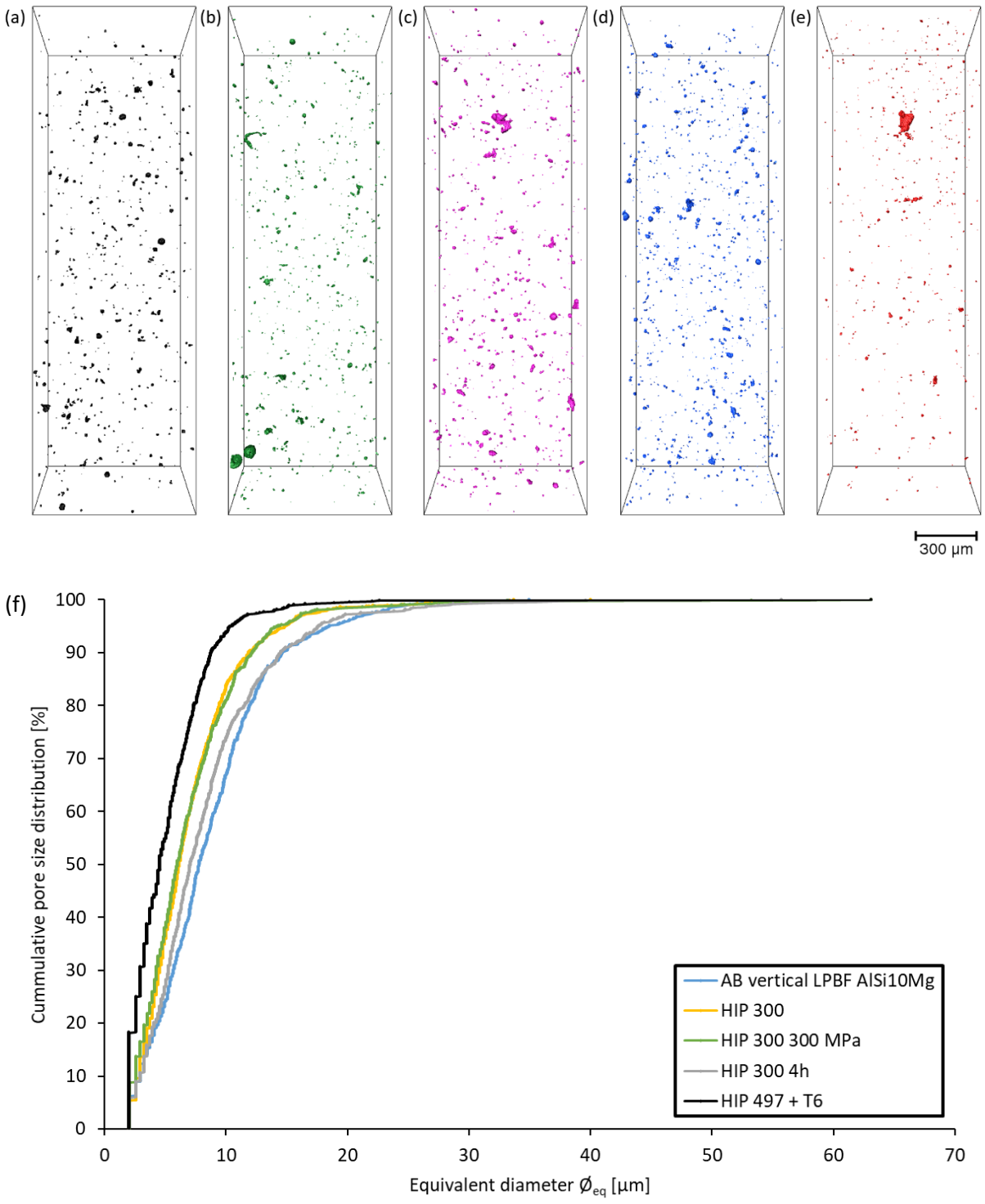

Fig. 6 3D depictions of porosity resulting from tomographies of LPBF AlSi10Mg samples in the following states: as built (a), HIP 300°C / 300 MPa / 2 h (b), HIP 300°C / 300 MPa / 4 h (c), HIP 300°C / 100 MPa / 2 h (d), HIP 497°C / 100 MPa / 2 h + T6 (e); cumulative pore size distribution for said states (f)

The HIP post-treatment at 300°C results in porosity increase. Fig. 2 shows that the slight porosity difference between the various HIP treatments at 300°C (Table 2) cannot really be associated to the dwell time (2 or 4 hours) or the applied pressure (100 or 300 MPa) but should rather be attributed to the local presence of a limited number of large porosities in the small analysed volume. Indeed, large porosities as found in Fig. 6b,c significantly drive the porosity value. As a conclusion, it may be said that the 300°C HIP treatment presents little interest for porosity reduction regardless of the pressure or process time.

Table 2. Porosity from X-ray tomography data.

Denomination	Porosity
AB	0.043 %
HIP 300	0.066 %
HIP 300 - 4 h	0.059 %
HIP 300 - 100 MPa	0.052 %
HIP 350	0.0004 % (Upper) / 0 % (Lower)
HIP 497	0 %
HIP 497 + HT	0.0215 %

At 350°C and 497°C porosity is reduced to an undetectable level, that is at the tomography resolution of 1.66 µm, in consonance with the simulation results presented in Fig. 2. The HIP 350 data is systematic and reproducible, showing extremely limited differences between the two scanned volumes. The 0.0004% detected in the upper volume could be considered not significant and even be attributed to artefacts or noise. Interestingly, the T6 heat treatment after HIP at 497°C leads to detection of porosity, which evidently appeared due to the 540°C solution treatment, similarly to what Hastie et al. [19] observed. The porosity level is approximately half of that of the AB material, but, in the analysed tomography volume, a significantly large pore ($Ø_{eq}$ = 22.4 µm), which could have an important negative effect in fatigue behaviour, was detected (see Fig. 6e,f).

Following the porosity level results of Table 2, only the 350°C and 497°C HIP treatments were considered for further characterisation.

4.2. Si-rich phase microstructure

The typical fine microstructure of as built LPBF AlSi10Mg can be appreciated in Fig. 7a. It is formed by a Si-rich eutectic network that surrounds α-Al cells, inside which fine Si precipitates are observed, as extensively characterised in 3D in previous work with the same LPBF processing conditions [2]. After HIP at 497°C the initial microstructure is significantly coarsened, the network is disintegrated and the fine Si precipitates are dissolved. Note the presence of large Si-rich eutectic particles in Fig. 7b.

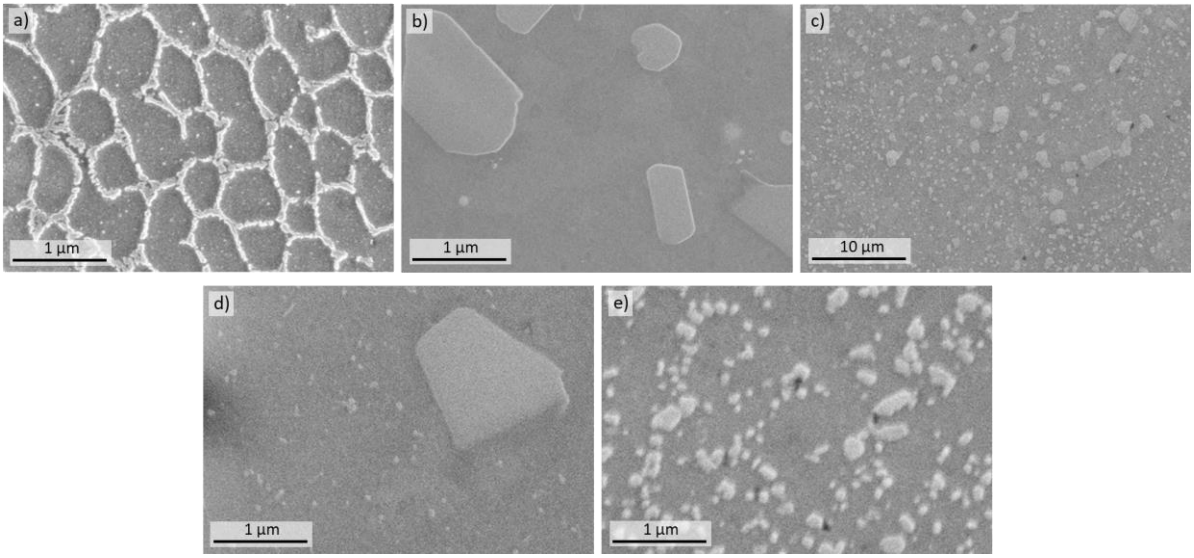

Fig. 7 SEM micrographs of LPBF AlSi10Mg for AB (a), HIP at 497°C (b,c), HIP at 497°C + T6 (d) and HIP at 350°C (e) states

A subsequent T6 heat treatment produces growth of the Si-rich eutectic particles and reprecipitation of fine Si-rich particles, as pictured in Fig. 7d. Precipitates such as β'' can also be formed, leading to partial recovery of strength, as demonstrated by Zhou et al [29]. HIP at 350°C also produces a network disintegration effect, noticeable in Fig. 7e, but the fineness of the microstructure is better preserved. Porosity is still visible under SEM after both HIP at 497°C and 350°C, as observable in Fig. 7c,e, but its size is very small and it is thus undetected by X-ray tomography.

In what follows, mechanical characterisation will only focus on the most promising HIP conditions, i.e. HIP 350 and HIP 497 (with and without T6). They will be compared to the as built condition.

4.3. Tensile properties

Representative true and engineering stress-strain curves are provided in Fig. 8 and supplementary Fig. 2, respectively. The strain at failure is calculated as $\varepsilon_f = \ln (A_0/A_f)$, where A_0 is the initial section area of the specimen and A_f is the section area at failure. Together with the stress at failure $\sigma_f = F_f/A_f$, these calculations allow to plot the last point of the curves, represented by a cross in Fig. 8. The discontinuous line is a linear extrapolation representing the material's behaviour after necking.

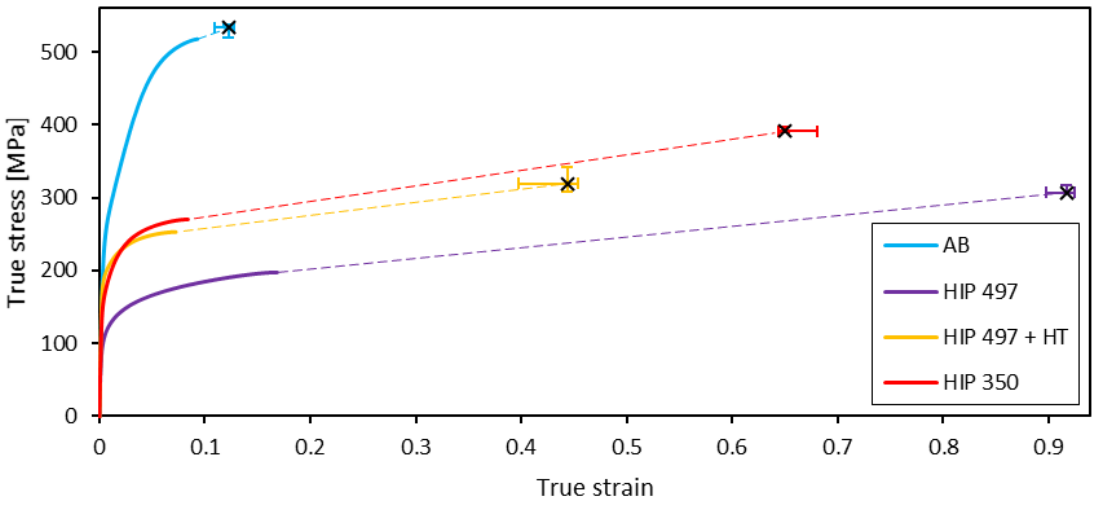

Fig. 8 Representative true stress-strain curves of LPBF AlSi10Mg under AB, HIP at 497°C, HIP 497 + HT and HIP 350 conditions

As expected based on the globularised and coarsened microstructure (Fig. 7) and the work of Zhao et al. [3], high temperature heat treatments lead to loss of strength compared to the as built conditions, associated with significant ductility increase. These results show that the 350°C HIP treatment is an excellent compromise. Indeed, by only applying the 350°C HIP (one step treatment), the outcome is similar strength and better ductility than the 497°C HIP followed by HT (three step process), requiring thus no additional heat treatment.

The SEM characterisation of the longitudinal mid-section of the more relevant states is presented in Fig. 9. Damage in the AB condition occurs in the form of numerous small fractures at the Si-rich eutectic network (Fig. 9a).

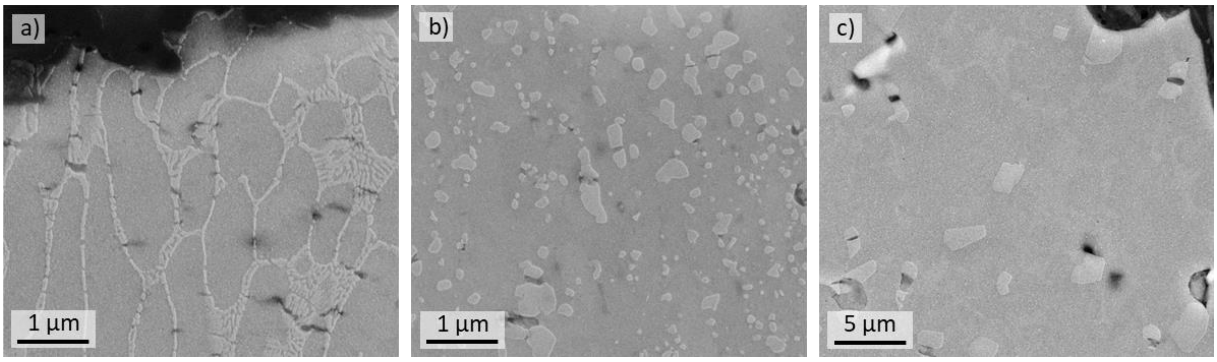

Fig. 9 SEM micrographs of longitudinal midsection at failure surface for AB (a), HIP 350 (b) and HIP 497 + HT (c) states

In the case of HIP states, damage events take place through fracture of Si-rich eutectic particles and decohesion between these particles and the α-Al matrix. These events are more numerous and smaller in size for the HIP 350 (Fig. 9b) condition compared to the HIP 497 + HT (Fig. 9c) one.

4.4. Fatigue properties

Fig. 10a shows the fatigue Wöhler curves for AB, HIP 497 + HT and HIP 350 samples. σ_{max} is the maximum stress during the dynamic loading. The arrowed point indicates a run-out sample. These results demonstrate that even if pores are closed by the HIP treatment at 350°C and 300 MPa for 2 hours and its fatigue resistance is superior to the HIP 497 + HT, this is not sufficient to improve the fatigue life compared to the as built conditions. Now, if HIP has to be applied in structural aerospace parts in order to ensure microstructure homogenisation and higher ductility, the new 350°C HIP treatment is a promising single step alternative to the HIP 497 + HT involving two additional steps. The yield stress weighted Wöhler curves represented on Fig. 10b show the positive effects of the HIP 350 process, since the samples for that condition show the best behaviour compared to the AB and HIP 497 + T6 specimens. This can be well rationalised by the porosity reduction after HIP at 350°C. The lower scatter of the HIP 350 data evidences the significant porosity present in the AB and HIP 497 + HT materials that will influence each sample more or less severely depending on the specific position of the critical pore with regard to other defects and the surface. Fig. 10b evidences well the behaviour similarity of the AB and HIP 497 + T6 states.

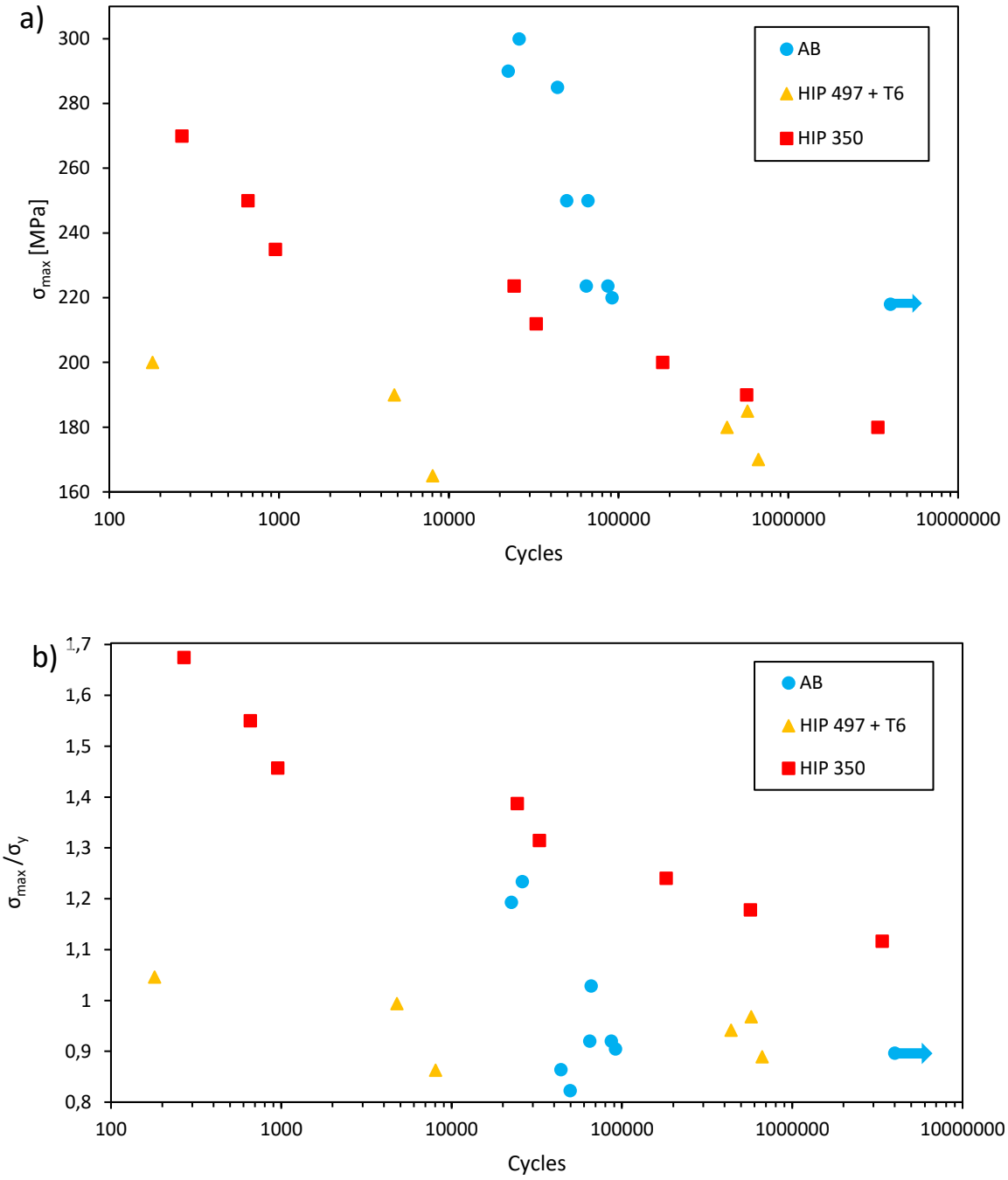

Fig. 10 Wöhler (a) and yield stress weighted Wöhler (b) curves of LPBF AlSi10Mg under AB, HIP 497°C + HT and HIP at 350°C conditions. The arrowed points represent a run-out

Fractography imaging was performed on samples after fatigue failure. The fatigue crack nucleation site of an as built sample is shown in Fig. 11a, where a critical defect, a pore, can be observed. A detail of this porosity of equivalent diameter around 20 µm is observable in Fig. 11b. A defect can also be observed at the nucleation site of a HIP 497°C + T6 sample (Fig. 11c,d). Note that such porosities are indeed detected by tomography (Fig. 6). The fatigue crack

nucleation site of a HIP 350 sample is observable in Fig. 11e. Note the similar magnification for Fig. 11b,d,e allowing to compare the size of the defect at the fatigue crack nucleation site. The defect in the AB specimen is the largest, followed closely by the one in the HIP 497°C + T6, the HIP 350 °C one being significantly smaller. A detail of the defect leading to the fatigue crack is provided in Fig. 11f. A very slight crack can be observed in the bottom of this porosity.

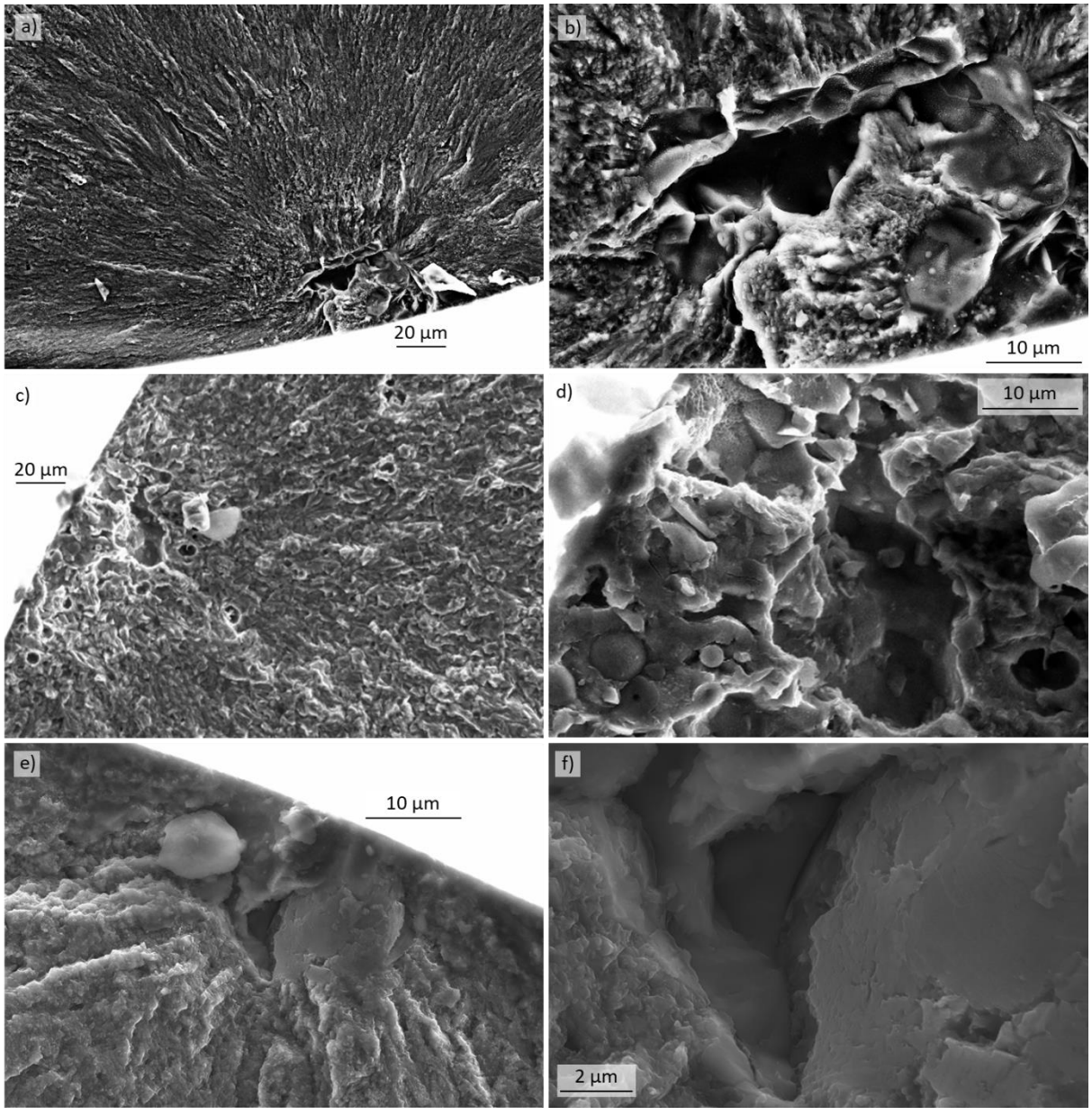

Fig. 11 Representative fatigue fractography SEM micrographs of LPBF AlSi10Mg for AB (a,b) HIP at 497°C + T6 (c,d) and HIP at 350°C (e,f) states. b,d,e, are zooms of a,c,e, respectively. Maximum stress is 250 MPa (a,b), 180 MPa (c,d) and 200 MPa (e,f)

In an attempt to improve the total fatigue life of the HIP 350 material, heat treatments were performed after said thermomechanical process. None of the tested artificial ageing treatments, 200°C during 8h or 160°C during 3h, 4h, 5h, 6h, 7h, 8h, 9h or 57h, resulted in a significant hardness improvement. Thus, no further mechanical testing was performed.

5. Discussion

AB LPBF AlSi10Mg presents a relatively high density level above 99.5% (see Table 2), but according to Fig. 11a,b there is some rather large size porosity responsible for fatigue crack nucleation and, consequently, for a decrease in total fatigue life. These defects are surely the compromising factor, since the AB material's strength is at a very satisfactory level (see Fig. 8). However, the amount and size of porosity and its homogeneous distribution almost guarantee the presence of a critical defect in the superficial region, more delicate for the higher stress intensity factor [3,30].

The porosity data from the tomography scans provide valuable information to discern which HIP parameters enable densification and which rather increase porosity. Indeed, the applied temperature can be too low for the necessary driving force for pore closure to be reached. This appears to be happening in the 300°C HIP treatments according to Table 2, which even shows a slight increase of porosity. Indeed, it could be that, at those conditions, there is not enough driving force for porosity closure, but diffusion of hydrogen metastably trapped in the microstructure is taking place, resulting in porosity increase [31]. These parameter sets thus allow a deleterious effect to take place, while the positive one is not happening.

The finite element simulations (see Fig. 2) identify an effect of the pressure on the porosity even at 300°C. This could not be clearly evidenced within the experimental results of Table 2 possibly due to the lack of representativeness of the sample, since the presence of scarce large pores influences the total porosity data at a significant enough level to hinder parameter influence analysis. In addition, the porosity increase, possibly due to metastably trapped hydrogen, is not accounted for in the finite element simulation.

The X-ray tomography results show that a 50°C increase in temperature (350°C HIP) provides enough driving force for pore closure. This correlates impressively well with the simulation of Fig. 2.

The tomography data for AB and HIP 350 assembled in Table 2 can be seen as signs of material and part homogeneity. The 0.0004% is not significant enough to draw conclusions, if not altogether negligible and similar to 0%. It could be attributed to the presence of some porosity in the AB material that was larger than normal and was not reduced to an undetectable level, or even to noise and artefacts related to the technique (mentioned in section 4.1).

Large pores are indeed a critical issue for AM and for the HIP treatment. They can originate from lack of fusion or trapped gas (hydrogen, argon, nitrogen, oxygen) during the AM process [32,33]. The irregular lack of fusion defects can be of very significant size, thus the difficulty to achieve complete closure of these pores. Large spherical trapped gas pores contain indeed gas that, when the HIP process reduces the pore size, and if diffusion is not possible, remains in the diminished space, increasing in pressure. This can act against the closure of the pore and eventually can help reopen it.

On the other hand, when the temperature is relatively low (i.e. lower than 350°C) or the isostatic pressure is not sufficiently high, the HIP induced local deformation will be limited and cannot effectively close large pores.

Logically the 497°C HIP also densifies LPBF AlSi10Mg. It is worth noting that although the tomography detects no porosity, small pores are observable by SEM (patent in Fig. 7c,e), indicating that full densification is not achieved by any of the studied HIP conditions. Moreover, as can be appreciated in Fig. 7b, the high temperature has a very severe coarsening effect, aside from the network breakdown. This translates into a very high ductility, but also leads to such a critical depletion of the material's strength (see Fig. 8) that the potential performance improvement under cyclic load from densification is countered. Thus, the 497°C HIP material is not expected to have a better total fatigue life than AB LPBF AlSi10Mg. A heat treatment to restore part of the lost strength can be envisaged as a solution. The solution and ageing treatment almost doubles the strength after HIP, halving fracture strain at the same time. This strength increase is mainly due to the appearance of fine Si-rich precipitates observable in Fig. 7d. The lower ductility is due to the presence of large Si-rich eutectic particles that are damage prone sites. The T6 treatment does not allow to reach the performance of HIP 350.

The heat treatment following HIP increases the porosity level. Reopening of closed porosity could be taking place. The reappearance of significantly large porosity, although not reaching the level of the AB material, could explain the fatigue underperformance. The fact that there are less large pores could also justify the occurrence of less aligned data points (i.e. more scatter

or dispersion of the fatigue data) for the HIP 497 + HT condition depicted in Fig. 10, as compared to the other two curves. Note that in the AB case there are more large pores, which implies a more constant distribution in the material, hence more stable fatigue performance. In the HIP 350 state no occurrence of large porosity was detected, which could explain the smoother curve, since it cannot be affected by the eventual presence of a more or less critical pore in a more or less critical site.

Compared to the as built state, all of the studied HIP conditions decrease the strength, as Fig. 8 manifests. They also provide a significant ductilisation effect. The reduction in strength is mainly linked to the growth and associated lower strengthening contribution of the fine (nanometric scale) Si-rich precipitates when the alloy is subjected to a post-treatment, as comprehensively discussed by [2,3,34].

The fatigue testing shows no improvement of total fatigue life after HIP at 497°C followed by T6 heat treatment nor after HIP at 350°C and 300 MPa during 2 h (see Fig. 10a). This is probably due in part to the strength depletion (otherwise, as Fig. 10b shows, HIP 497 + T6 is not as negative and HIP 350 is a positive treatment) and to the remaining presence of porosity (see Fig. 11c-f). Indeed, the porosity could be only partially closed (i.e. no or insufficient metallurgical fusion) after HIP and reopen again under fatigue loading with relative ease. Indeed, Finfrock et al. [15] and Larrosa et al. [18] have showed that pancake-like cracks are still present even after a higher temperature (521°C and 500°C respectively) HIP treatment. These cracks are likely to reopen during loading. It is therefore necessary to try to improve the current HIP parameters, since porosity reduction does not seem to suffice. The HIP treatment might be so severe that too much strength is lost. A lower dwell time could possibly reduce the effect of the treatment in the microstructure, allowing for lower strength reduction. Indeed, according to our simulation results, the porosity reduction mainly occurs upon application of temperature and pressure, while the contribution of creep flow is relatively low.

It must be noted that the as built material does not present significant anisotropy in fatigue resistance, as a comparison between the data introduced in this work and that presented in Santos Macías et al. [5] attests (see supplementary Fig. 3). This could signal that porosity, although still naturally playing a central role in fatigue behaviour, is at a lower level of negative influence compared to other publications dealing with the same material, where significant differences between horizontal and vertical fatigue testing were observed. This could mean that the partial porosity reduction effect brought about by HIP, as presented in this research, is less pronounced than it could be for a more porous material, especially if it presented significant

lack of fusion defects, more anisotropic and eventually larger than trapped gas ones. Furthermore, this effect has to be sized up against that of strength reduction.

The possibility of performing heat treatments following HIP at 350°C and 300 MPa during 2 h was explored, but no significant mechanical behaviour improvement was obtained with any of the 200°C or 160°C temperatures. This might be due to the fact that 350°C is not sufficient to dissolve Si phase which is necessary for subsequent precipitation. Further research could be performed with relatively higher temperature (above 400°C) and lower dwell time (10 min for example) HIP, followed by ageing, to achieve even more positive results.

6. Conclusion

In this work, a set of HIP parameters (350°C, 300 MPa, 2 h) involving a much lower temperature than the conventional one around 500°C while still producing similar densification has been identified. This confirms the trends observed in the finite element simulations. Moreover, this new set of parameters has a much higher strength than the classic one, with a slightly lower ductility. Its performance is even better than that of the conventional HIP after solution and ageing heat treatment. In addition, this new HIP strategy only requires one HIP step without any additional post-HIP heat treatments.

This research has also shown that the role of the temperature parameter is dominant and a minimum temperature above 300°C is necessary to reach the critical driving force level for pore closure. A minimum pressure of 150 MPa is also required.

To achieve total fatigue life improvement, further optimisation is necessary, probably focusing on lower dwelling time to reduce the impact on microstructure and strength, and higher temperature to enable subsequent ageing recovering mechanical strength.

Acknowledgements

The authors acknowledge the support of Guillaume Contzen, Azziz Hocini and Nathan Wiertz.

Compliance with ethical standards

Funding: JGSM acknowledges the support of the Fonds de la recherche scientifique – FNRS (FRIA grant), Belgium. This research has also been funded (from January 2017) by the European research council (ERC) under the European Union's Horizon 2020 research and innovation program (grant agreement n°716678). This research work has also been supported from January 2019 by the WALInnov LongLifeAM project, convention n°1810016, funded by the service public de Wallonie économie emploi recherche (SPW-EER).

Conflict of interest: The authors declare that they have no conflict of interest.

References

[1] Leary M (2019) Design for additive manufacturing. Elsevier

[2] Santos Macías JG, Douillard T, Zhao L, Maire E, Pyka G, Simar A (2020) Influence on microstructure, strength and ductility of build platform temperature during laser powder bed fusion of AlSi10Mg. Acta Mat 201:231-243

[3] Zhao L, Santos Macías JG, Ding L, Idrissi H, Simar A (2019) Damage mechanisms in selective laser melted AlSi10Mg under as built and different post-treatment conditions. Mater Sci Eng A 764:138210.

[4] Santos Macías JG, Elangeswaran C, Zhao L, Van Hooreweder B, Adrien J, Maire E, Buffière JY, Ludwig W, Jacques P, Simar A (2019) Ductilisation and fatigue life enhancement of selective laser melted AlSi0Mg by friction stir processing. Scr Mater 170:124-128

[5] Santos Macías JG, Elangeswaran C, Zhao L, Buffière JY, Van Hooreweder B, Simar A (2021) Fatigue crack nucleation and growth in laser powder bed fusion AlSi10Mg under as built and post-treated conditions. Mater Des 210:110084

[6] Romano S, Beretta S, Brandão A, Gumpinger J, Ghidini T (2017) HCF resistance of AlSi10Mg produced by SLM in relation to the presence of defects. Procedia Struct Integr 7:101-108

[7] Romano S, Brandão A, Gumpinger J, Gschweitl M, Beretta S (2017) Qualification of AM parts: Extreme value statistics applied to tomographic measurements. Mater Des 131:32-48

[8] Nadot Y, Nadot-Martin C, Kan WH, Boufadene S, Foley M, Cairney J, Proust G, Ridosz L (2019) Predicting the fatigue life of an AlSi10Mg alloy manufactured via selective laser melting by using data from computed tomography. Addit Manuf 32:100899

[9] Atkinson HV, Davies S (2012) Fundamental aspects of hot isostatic pressing: An overview. Metall Mater Trans A 31(12):2981-3000

[10] Chastand V, Quaegebeur P, Maia W, Charkaluk E (2018) Comparative study of fatigue properties of Ti-6Al-4V specimens built by electron beam melting (EBM) and selective laser melting (SLM). Mater Charact 143:76-81

[11] Rosenthal I, Tiferet E, Ganor M, Stern A (2015) Post-processing of AM-SLM AlSi10Mg specimens: mechanical properties and fracture behaviour. Galaty Univ Press

[12] Hirata T, Kimura T, Nakamoto T (2020) Effects of hot isostatic pressing and internal porosity on the performance of selective laser melted AlSi10Mg alloys. Mater Sci Eng A 772:138713

[13] Rosenthal I, Shneck R, Stern A (2018) Heat treatment effect on the mechanical properties and fracture mechanism in AlSi10Mg fabricated by additive manufacturing selective laser melting process. Mater Sci Eng A 729:310-322

[14] Uzan NE, Shneck R, Yeheskel O, Frage N (2017) Fatigue of AlSi10Mg specimens fabricated by additive manufacturing selective laser melting (AM-SLM). Mater Sci Eng A 704:229-237

[15] Finfrock CB, Exil A, Caroll JD, Deibler L (2018) Effect of hot isostatic pressing and powder feedstock on porosity, microstructure, and mechanical properties of selective laser melted AlSi10Mg. Metall Microstruct Anal 7:443-456

[16] Tradowsky U, White J, Ward RM, Read N, Reimers W, Attallah MM (2016) Selective laser melting of AlSi10Mg: Influence of post-processing on the microstructural and tensile properties development. Mater Des 105:212-222

[17] Ertuğrul O, Öter ZÇ, Yılmaz MS, Şahin E, Coşkun M, Tarakçı G, Koç E (2020) Effect of HIP process and subsequent heat treatment on microstructure and mechanical properties of direct metal laser sintered AlSi10Mg alloy. Rapid Prototyp J 26:1421-1434

[18] Larrosa NO, Wang W, Read N, Loretto MH, Evans C, Carr J, Tradowsky U, Attallah MM, Withers PJ (2018) Linking microstructure and processing defects to mechanical properties of selectively laser melted AlSi10Mg alloy. Theor Appl Fract Mech 98:123-133

[19] Hastie JC, Kartal ME, Carter LN, Atallah MM, Mulvihill DM (2020) Classifying shape of internal pores within AlSi10Mg alloy manufactured by laser powder bed fusion using 3D X-ray micro computed tomography: Influence of processing parameters and heat treatment. Mater Charact 163:110225

[20] Hastie JC, Koelblin J, Kartal ME, Attalah MM, Martinez R (2021) Evolution of internal pores within AlSi10Mg manufactured by laser powder bed fusion under tension: As-built and heat treated conditions. Mater Des 204:109645

[21] Kan WH, Nadot Y, Foley M, Ridosz L, Proust G, Cairney JM (2019) Factors that affect the properties of additively manufactured AlSi10Mg: Porosity versus microstructure. Addit Manuf 29:100805

[22] Schneller W, Leitner M, Leuders S, Sprauel JM, Grün F, Pfeifer T, Jantschner O (2020) Fatigue strength estimation methodology of additively manufactured metallic bulk material. Addit Manuf 39:101688

[23] Schneller W, Leitner M, Springer S, Grün F, Taschauer M (2019) Effect of HIP treatment on microstructure and fatigue strength of selectively laser melted AlSi10Mg. J Manuf Mater Process 3:16

[24] Tocci M, Pola A, Gelfi M, La Vecchia GM (2020) Effect of a new high-pressure heat treatment on additively manufactured AlSi10Mg alloy. Metall Mater Trans A 51A:4799-4811

[25] Giovagnoli M, Tocci M, Fortini A, Merlin M, Ferroni M, Migliori A, Pola A (2021) Effect of different heat-treatment routes on the impact properties of an additively manufactured AlSi10Mg alloy. Mater Sci Eng A 802:140671

[26] ABAQUS/Standard User's Manual. Providence, RI, (2016)

[27] Uzan NE, Shneck R, Yeheskel O, Frage N (2018) High temperature mechanical properties of AlSi10Mg specimens fabricated by additive manufacturing using selective laser melting technologies (AM-SLM). Addit Manuf 24:257-263

[28] EOS GmbH - electro optical systems, Material data sheet for EOS aluminium AlSi10Mg, München, 2014

[29] Zhou L, Mehta A, Schulz E, McWilliams B, Cho K, Sohn Y (2018) Microstructure, precipitates and hardness of selectively laser melted AlSi10Mg alloy before and after heat treatment. Mater Charact 143:5-17

[30] Murakami Y (2019) Metal fatigue: Effects of small defects and nonmetallic inclusions 2nd ed. Elsevier, Oxford

[31] Delroisse P (2018) AlSi10Mg lattice structures produced by selective laser melting: from microstructure characterization to impact resistance. PhD Dissertation, Université catholique de Louvain

[32] Kan W, Nadot Y, Foley M, Ridosz L, Proust G, Cairney JM (2019) Factors that affect the properties of additively manufactured AlSi10Mg: Porosity versus microstructure. Addit Manuf 29:100805

[33] Galy C, Guen EL, Lacoste E, Arvieu C (2018) Main defects observed in aluminum alloy parts produced by SLM: From causes to consequences. Addit Manuf 22:165-175

[34] Wu H, Ren Y, Ren J, Liang L, Li R, Fang Q, Cai A, Shan Q, Tian Y, Baker I (2021) Selective laser melted AlSi10Mg alloy under melting mode transition: Microstructure evolution, nanomechanical behaviors and tensile properties. J Alloy Compd 873:159823